RESEARCH ARTICLE

Diurnal variations of the meridional overturning circulations over West Africa during the premonsoon and monsoon seasons

Lidia Huaman[1,2] | Courtney Schumacher[1] | Andreas H. Fink[3] | Erin Buttitta[1]

[1]Department of Atmospheric Sciences, Texas A&M University, College Station, Texas, USA

[2]Data and Weather Technology, AccuWeather Inc., State College, Pennsylvania, USA

[3]Institute of Meteorology and Climate Research, Karlsruhe Institute of Technology, Karlsruhe, Germany

Correspondence
Lidia Huaman, Data and Weather Technology, AccuWeather Inc., State College, PA, USA.
Email: lidia.huaman@accuweather.com

Abstract

Diurnal variations in the shallow and deep meridional overturning over West Africa during the premonsoon (April–May) and monsoon (July–September) seasons were analyzed using ECMWF Reanalysis 5th Generation (ERA5) reanalysis and *Tropical Rainfall Measuring Mission* (*TRMM*)/*Global Precipitation Measurement* (*GPM*) satellite radar data from 1998 to 2019. We found that a daytime sea breeze and two nocturnal low-level jets have varying impacts on the diurnal cycle of convection and the meridional circulations over West Africa, depending on the season. During the premonsoon, the zonal rain belt is centered over the Gulf of Guinea and the sea breeze initiates intense deep convection (and thus deep overturning) over the coastal region in the afternoon that propagates northward into the early evening. The nocturnal Sahel/Sahara low-level jet (SLLJ) then drives low-level convergence into the West African heat low, producing a strong, dry shallow overturning over land at night. During the monsoon, the rain belt is centered over land (10°N) and the sea breeze is forced by weaker temperature gradients, producing less intense convection that does not propagate as far inland as during the premonsoon. However, organized convection inland maintains deep daytime overturning. At night, a coastal low-level jet strengthens northward moisture transport from the Gulf of Guinea into the active monsoon region after the sea breeze dissipates, helping maintain convective systems with large stratiform components and continued deep meridional overturning over land. The nocturnal SLLJ still drives low-level convergence into the West African heat low, but the dry shallow meridional overturning is farther north and weaker than in the premonsoon. While ERA5 winds and moisture-flux convergence are generally consistent with diurnal variations in the *TRMM*/*GPM* precipitation, ERA5 precipitation is not. The reanalysis indicates significant biases in the timing and magnitude of rainfall over the Gulf of Guinea and West Africa in each season, with the convective and large-scale rain fields both contributing to the disparate precipitation patterns.

KEYWORDS

African monsoon, low-level jet, meridional circulation, sea breeze

1 | INTRODUCTION

The shallow and deep meridional overturning circulations over West Africa vary seasonally (e.g., Trenberth *et al.*, 2000; Zhang *et al.*, 2006; Thorncroft *et al.*, 2011; Johnson and Ciesielski, 2020). During the premonsoon season (boreal spring), organized convective systems and deep meridional overturning are predominant offshore in the Gulf of Guinea. During the monsoon season (boreal summer), shallow and midlevel nonprecipitating stratiform clouds dominate offshore in the Gulf of Guinea (Fink *et al.*, 2017), while maximum thunderstorm activity and its associated deep overturning occur further inland. A shallow meridional circulation (SMC) is observed to the north of the main precipitation region during both seasons and its shallow return flow penetrates into the latitude of deep convection to the south (Zhang *et al.*, 2008; Martin and Thorncroft, 2014; Shekhar and Boos, 2017). The upward motion of the SMC is associated with the West African heat low, which predominates near the surface (Lavaysse *et al.*, 2009), and precipitation is inhibited over this region. The West African heat low is over the Sahel during the premonsoon and moves northward over the Sahara desert during the monsoon. While the focus of this study is on variations in meridional overturning structures, it should be noted that an anticyclonic circulation predominates above the West African heat low around 700 hPa and produces strong easterly flow on its flank known as the African easterly jet. The combination of the strong meridional thermal and soil moisture contrasts and dry convection in the West African heat low is crucial to maintain the jet (Thorncroft and Blackburn, 1999).

Although a number of studies have discussed how precipitation and meridional winds vary throughout the day and night over the region (Sultan *et al.*, 2007; Vondou *et al.*, 2010; Bouniol *et al.*, 2012; Gounou *et al.*, 2012; Janiga and Thorncroft, 2014; Collow *et al.*, 2016; Pfeifroth *et al.*, 2016; Laing *et al.*, 2018; Liu *et al.*, 2019; Vizy and Cook, 2019; Liu *et al.*, 2020), diurnal variations in the shallow and deep meridional overturning circulations over West Africa and their associated convection have not been addressed extensively in the literature. A major goal of this study is to explain how these variations contribute to the daily evolution of the shallow and deep meridional overturning over West Africa before and after monsoon onset.

During the day over West Africa, a late afternoon precipitation maximum occurs away from topography after daytime heating has destabilized the lower troposphere (Zhang *et al.*, 2016). There is also a daytime sea breeze circulation related to the differential heating of the ocean and land surface and the resulting strong meridional temperature and density gradients near the Gulf of Guinea coastal zone. The northward propagating sea breeze is most frequent in boreal winter, but can be observed throughout the year (Guedje *et al.*, 2019). Shallow convective showers cross the coastline during morning hours and develop into strong afternoon thunderstorms while propagating inland (Maranan *et al.*, 2018). Fink *et al.* (2010) found substantial rainfall associated with the sea breeze circulation between March and November.

An additional late evening rain maximum occurs over West Africa during the monsoon season (e.g., Yang and Slingo, 2001). This is the time when mesoscale convective systems contribute the most rain over the region (Nesbitt and Zipser, 2003). Parker *et al.* (2005) also observed a nighttime intensification of low-level southerly winds inland over West Africa during boreal summer, which was later documented as a nocturnal low-level jet by Lothon *et al.* (2008). We label this wind feature the Sahel/Sahara low-level jet (SLLJ), because it is located over the Sahel during the premonsoon season and the Sahara during the monsoon season. Fiedler *et al.* (2013) found that the SLLJ is stronger and more frequent from May to July and can impact dust emissions throughout the year. A separate nocturnal coastal low-level jet (CLLJ) was reported by Guedje *et al.* (2019) over Benin during the monsoon season. The CLLJ is important for the northward transport of cold air with high relative humidity and nighttime genesis of extensive stratus cloud (Lohou *et al.*, 2020). It is worth mentioning that the impacts of the sea breeze, SLLJ, and CLLJ on the overturning meridional circulations and associated convection have not been addressed synergistically in the literature.

The main objective of this study is to characterize the diurnal variation of West African shallow and deep overturning meridional circulations and determine the impacts of the sea breeze, SLLJ, and CLLJ on the diurnal cycle of convection during the premonsoon season in April, May, and June (AMJ) and the monsoon season in July, August, and September (JAS) using ECMWF Reanalysis 5th Generation (ERA5) reanalysis fields and precipitation observations from the National Aeronautics and Space Administration (NASA) *Tropical Rainfall Measuring Mission* (*TRMM*) and *Global Precipitation Measurement* (*GPM*) satellite radars. ERA5 has an advanced assimilation system and the highest temporal and spatial resolution available amongst modern reanalyses with which to study the diurnal cycle over the West African region. In addition, the *TRMM*/*GPM* radars are capable of differentiating precipitation by type (i.e., shallow and deep convection and stratiform), which can be linked more directly to shallow and deep overturning. As climate models have trouble representing the diurnal cycle of precipitation, potentially due to the fidelity of their convective parameterizations and relatively coarse temporal and horizontal resolutions

(Diro *et al.*, 2012), this work will also shed light on the importance of representing diurnal variability in order to capture accurate seasonal mean meridional overturning and its associated energetics over West Africa (e.g., Vizy and Cook, 2002). This article is organized as follows. Section 2 presents the data and methodology. Section 3 describes ERA5 and *TRMM/GPM* seasonal conditions, followed by the diurnal cycle of dynamic fields from ERA5 in Section 4. The diurnal cycle of precipitation from ERA5 and the *TRMM/GPM* radars is in Section 5, a synthesis of mechanisms is discussed in Section 6, and conclusions are provided in Section 7.

2 | DATA AND METHODOLOGY

Hourly data from ERA5 (Hersbach *et al.*, 2020) for 1998–2019 were used in this study. ERA5 has 37 vertical pressure levels and a horizontal resolution of 32 km. We interpolated the data to 0.5° using bilinear interpolation to match the resolution of the *TRMM/GPM* data. This resolution captures the large-scale shallow and deep meridional circulations well, as well as the sea breeze and low-level jet features. Recent studies have shown small biases in ERA5 winds over West Africa compared with observations (Van der Linden *et al.*, 2015). Additionally, ERA5 represents the wind-field variability over this region better compared with other reanalyses (Foli *et al.*, 2022). ERA5's high temporal resolution also allows analysis of the diurnal variation of winds over the West African region with higher fidelity than previously available reanalyses, which have three-hourly or coarser resolution. The ERA5 variables used in this study were horizontal and vertical winds, temperature, humidity, vertically integrated moisture divergence (VIMD), and large-scale and convective precipitation. The precipitation is from a short-term forecast, while the other variables come from the analysis. The VIMD from ERA5 avoids the problem with orography and is integrated over the entire model column. This variable is highly related to moisture tendency and precipitation rate.

The sea breeze and nocturnal low-level jets were identified using meridional winds and convergence from ERA5 at 950 hPa. The sea breeze is identified by enhanced southerly flow and convergence originating over the coast that propagates inshore with a speed of around 10 m·s^{-1} between the late morning and afternoon (Grams *et al.*, 2010). The speed of the sea breeze can be calculated by dividing the convergence propagation distance by the time of the propagation. The CLLJ and SLLJ are identified by the enhanced southerly winds that produce convergence near the coast and between 15°N and 25°N, respectively, at night and early morning. The vertical structure

of ERA5 vertical velocity and meridional flow at different times during the day was analyzed in order to determine the role of the sea breeze and CLLJ near the coast and the SLLJ farther inland on the deep and shallow meridional circulations and associated convection. Further details are described in Section 4.

Hourly *TRMM/GPM* precipitation observations were considered in this study to complement the ERA5 data, since precipitation is one of the less constrained variables in reanalyses. We used observations from the *TRMM* Precipitation Radar (PR: (PR, Kummerow *et al.*, 1998) for 1998–2014 and from the *GPM* Dual-Frequency Precipitation Radar (DPR: (DPR, Hou *et al.*, 2014) for 2014–2019. The orbital data were assigned to grids with a horizontal resolution of 0.5° and temporal resolution of an hour. The *TRMM* PR was a single-wavelength (K_u-band) radar that operated at 13.8 GHz. Its minimum detectable reflectivity was 17 (18) dBz and it had a swath width of 240 (215) km before (after) 2001, when the satellite was boosted from 350 to 402.5 km in order to conserve fuel. The *GPM* DPR consists of a K_a-band radar operating at 35.5 GHz and a K_u-band radar operating at 13.6 GHz. The swath width is 245 km for the K_u-band channel, and 125 km for the K_a-band channel. The DPR's minimum detectable reflectivity is approximately 14 dBz. This study uses *TRMM* 2APR and *GPM* 2ADPR products (Stocker *et al.*, 2018). *TRMM* 2APR comprises the data reprocessed using the newer *GPM* algorithms and provides surface precipitation that is retrieved using the near-surface reflectivity.

The *TRMM/GPM* precipitation is categorized as convective, stratiform, or shallow in the 2APR and 2ADPR products. The convective classification refers to regions of deep active convection, where strong vertical air motions dominate, and precipitation particles increase in mass by coalescence and/or riming (Houze, 1989). The stratiform classification represents regions of aging convection, where weaker vertical motions dominate, and precipitation particles increase in mass by vapor deposition above the melting level (i.e., 0 °C: (Houze, 1997). The convective–stratiform separation algorithm determines whether the echo is convective or stratiform by examining the horizontal variability of the reflectivity (Steiner *et al.*, 1995) and its vertical profile (Awaka *et al.*, 2007). The shallow classification refers to echo tops lower than the climatological 0 °C level and is generally considered to form from convective processes in the Tropics (Kodama *et al.*, 2009; Funk, 2013). It is worth mentioning that *TRMM/GPM* surface precipitation agrees well with ground observations (Dembélé and Zwart, 2016; Cannon *et al.*, 2017; Adirosi *et al.*, 2021; Atiah *et al.*, 2020).

The *TRMM* and *GPM* satellites overlapped from April–September 2014 before *TRMM* began its slow descent. Because the DPR is more sensitive than the PR,

we compared observations from both radars during this overlapping period to determine the impact of sensitivity on the precipitation retrievals. The DPR retrieved 10% more shallow precipitation than the PR during the monsoon season (i.e., JAS). Shallow convection typically has very low rain rates, so the DPR should be able to sense more of the shallow population than the PR because of its higher sensitivity to lighter rain. However, the DPR retrieved 25% less shallow precipitation compared with the PR during the premonsoon season (i.e., AMJ) around the coastal area (5°N). DPR deep convective precipitation increased over this region, so we postulate that, because the DPR's increased sensitivity makes it able to sense higher echo tops than the PR, it is more likely to categorize congestus clouds as deep convective rather than shallow. We note that the horizontal structure and diurnal variation of precipitation from the *GPM* and *TRMM* radars are consistent, and our main results do not change when the *TRMM* and *GPM* datasets are analyzed independently.

3 | SEASONAL MEAN PRECIPITATION AND MERIDIONAL OVERTURNING

Figure 1 shows the seasonal mean precipitation from the *TRMM*/*GPM* radars and seasonal mean vertical motion and meridional flow from ERA5 over West Africa from 1998 to 2019. The premonsoon season is represented by AMJ and the monsoon season is represented by JAS. These seasonal definitions delineate conditions before and during the monsoon better compared with the more traditional March–April–May (MAM)/June–July–August (JJA) seasonal separation (Gu and Adler, 2004; Fink *et al.*, 2010). Figure 1 is meant to provide context for the diurnal variations analyzed in the following sections, and is consistent with the previous results on the seasonal variations over West Africa described in the introduction.

Figure 1a,b shows that the main band of precipitation is offshore during the premonsoon, whereas most of the rain during the monsoon is over land. While a significant amount of rain is still present off the west coast of West Africa during the monsoon season, our study is focused on the southern coast and central portion of West Africa and the meridional patterns therein. As such, the rest of this study will only show latitudinal cross-sections between 7°W and 3°E (i.e., the dashed lines in Figure 1a,b). This longitude range was chosen because the precipitation is zonally uniform over this region and the coastline does not vary much with latitude, as well as to minimize orographic influences from the higher topography and the very wet regions to the west and east. The rain types by latitude (Figure 1c,d) and the cross-sections of meridional

overturning (Figure 1e,f) indicate two distinct regions during both seasons: a deep, highly convective circulation just south of the coast in AMJ and north of the coast in JAS, and a shallow circulation, weakly precipitating, located farther inland. The surface convergence associated with the deep convective circulation is produced due to the strong sea-surface temperature between the ocean and African continent (Hall and Peyrille, 2006).

During AMJ, the premonsoon season, deep upward motion linked to the deep meridional overturning is located around 4°N (Figure 1e), with southerly flow at the surface and northerly flow at upper levels at its equatorward flank. Strong precipitation is linked to this deep upward motion (Figure 1a), and convective, stratiform, and shallow precipitation explain 55%, 35%, and 10% of the total precipitation at this latitude, respectively (Figure 1c). Additionally, shallow upward motion is located over the Sahel around 15°N, with the return flow of the overturning circulation penetrating the latitude of deep upward motion at mid levels (Figure 1e). The dynamical processes of the West African SMC are different from those of the SMCs in the East Atlantic and East Pacific (Zhang *et al.*, 2008; Huaman and Schumacher, 2018). The ascending motion of the shallow circulation is linked to surface sensible heat fluxes instead of latent heating from convection (Hagos and Zhang, 2010). The West African SMC is also strengthened by the enhanced low-level convergence associated with the SLLJ (Lothon *et al.*, 2008). The West African SMC transports some moisture far inland and moderate amounts of convective and stratiform precipitation are seen in the southern part of the SMC region from 10–15°N (Figure 1c).

During JAS, the monsoon season, the deep upward motion linked to the deep meridional overturning is now located over land, at around 10°N (Figure 1f). This deep circulation is associated with large total amounts of both convective and stratiform precipitation (Figure 1d). Additionally, the fraction of rain that is stratiform is larger (40%) than in the premonsoon (32%), consistent with Schumacher and Houze Jr (2006). Even though the shallow precipitation is insignificant over the monsoon region (i.e., 4%), it is predominant over the coastal area (Maranan *et al.*, 2018). This shallow precipitation is linked to a very shallow circulation with overturning meridional flow at 800 hPa (Figure 1f). Additionally, the generally dry shallow upward motion linked to the West African SMC is located farther north and over the Sahara (around 20°N) and is less intense but wider compared with the premonsoon season. The total shallow upward motion seems to be composed of isolated shallow upward cells between 16° and 26°N, probably forced by irregularities in the topography over this region (Figure 1b), since air above elevated terrain warms more quickly (Lavaysse *et al.*, 2009).
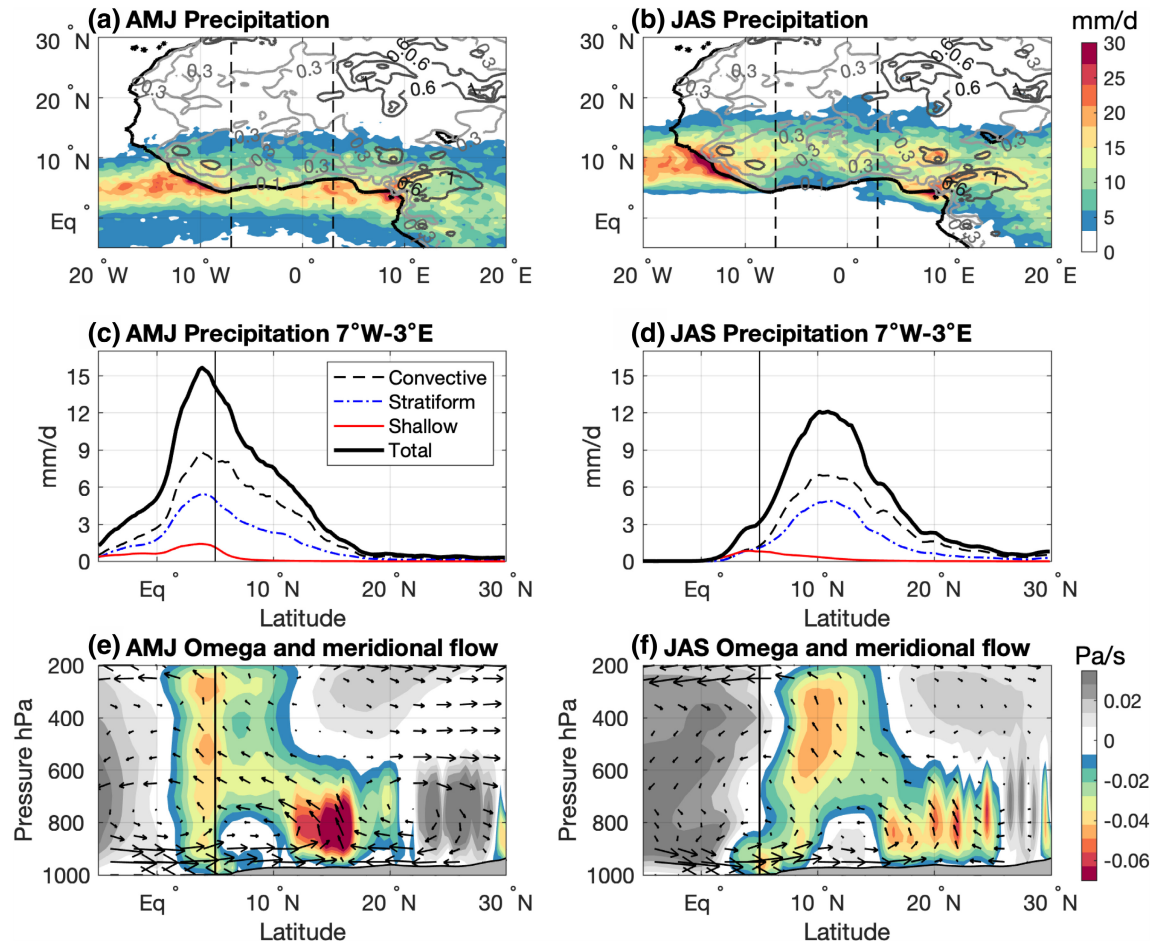
FIGURE 1 (a,b) Total precipitation from the *TRMM/GPM* radars (shaded, in mm·day^{-1}) and topography (contours, in km) during AMJ (left panel) and JAS (right panel). (c,d) Convective, stratiform, and shallow precipitation from *TRMM/GPM* radars and (e,f) omega cross-section (shaded, in Pa·s^{-1}) and meridional flow (arrows) from ERA5 across 7°W–3°E (dashed lines in top figures) for each season. The vertical meridional flow component has been multiplied by 10 to account for the small ratio of the plot. The largest meridional wind vector is 5 m·s^{-1}. The solid line at 5.5°N highlights the coastline. [Colour figure can be viewed at wileyonlinelibrary.com]

4 | DIURNAL CYCLE OF DYNAMICAL FIELDS

4.1 | Low-level features

The sea breeze and nocturnal low-level jets play important roles in the diurnal cycle of the West African region. During sea breeze events, the air over land warms during the daytime, pressure drops, and air accelerates from sea to land in response. Parker *et al.* (2005) and Lothon *et al.* (2008) explain the mechanisms behind the SLLJ and CLLJ as follows. In the daytime, the planetary boundary layer (PBL) is deep and the low-level winds are weak. This condition is associated with weak wind shear because of the vertical mixing with higher level winds. Overnight, the boundary layer becomes more stratified and turbulence is weaker, allowing winds just above the PBL (around 925 hPa) to strengthen. As the Coriolis force

is weak at lower latitudes, the wind acceleration during the night is proportional and parallel to the horizontal pressure gradient force associated with the West Africa heat low.

Figure 2 shows the seasonal cycle of the ERA5 950-hPa meridional wind (top panels) and divergence (bottom panels) in shading at different time periods of the day from 7°W–3°E. Since the sea breeze takes place during the afternoon and nocturnal low-level jets occur at night, an approximation of the sea breeze (nocturnal low-level jets) is calculated by removing the daily mean meridional wind and divergence from the 1200–1800 UTC (2000–0800 UTC) averages, shown as contours in Figure 2. We note that UTC and local time are indistinguishable in this longitude range. Wind anomalies of about 1 m·s^{-1} associated with the sea breeze occur over the coastal region (around 6°N) throughout the year (Figure 2a), and produce anomalies in low-level convergence (i.e., negative
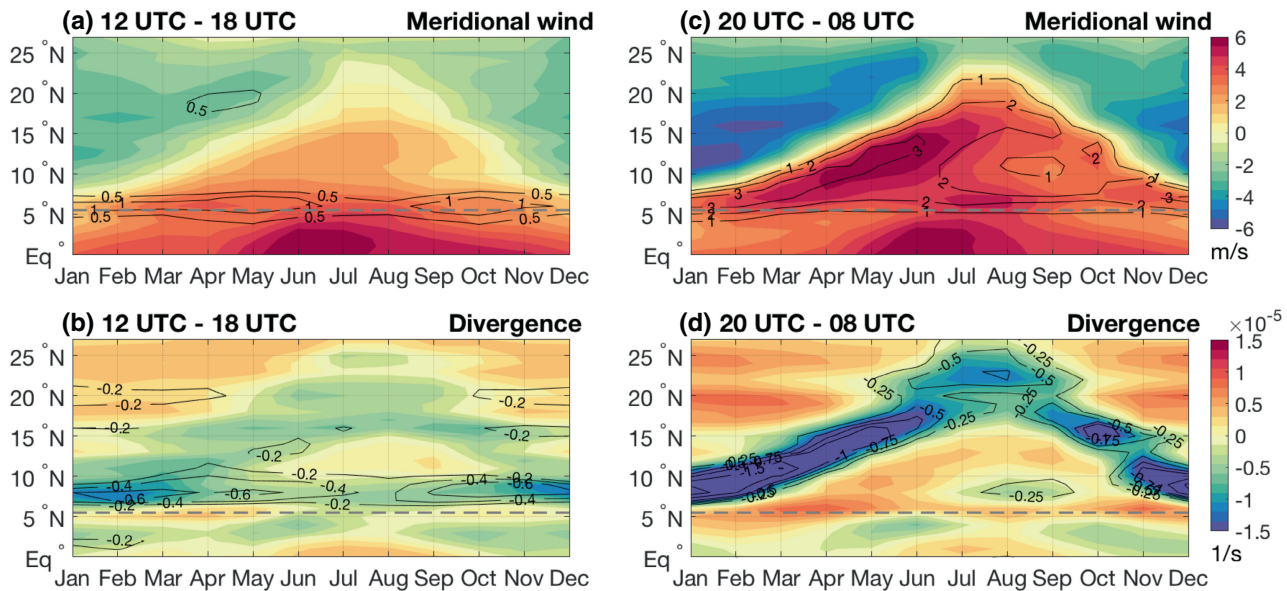
FIGURE 2 (a,c) Total meridional wind (shaded) and the sea breeze (1200–1800 UTC, contours) and nocturnal low-level jet (2000–0800 UTC, contours) anomalies in m·s^{-1} at 950 hPa, and (b,d) convergence (shaded) and sea breeze and nocturnal low-level jet anomalies (contours) in s^{-1} at 950 hPa. The dashed line at 5.5°N highlights the coastline. [Colour figure can be viewed at wileyonlinelibrary.com]

values of divergence) from 6–8°N that are strongest before and after the monsoon season (Figure 2b). The CLLJ is evident from July–September just north of the coast (around 8°N) in the low-level convergence field (Figure 2d). These sea breeze and CLLJ results are in agreement with the observational analysis over Benin done by Guedje *et al.* (2019), providing confidence in the ERA5 meridional wind structures over West Africa. The SLLJ is present farther north over land throughout the year, with the strongest wind anomalies during the premonsoon season (Figure 2c). The southerly flow of the SLLJ migrates between 5°N in winter and 20°N in summer and drives strong low-level convergence into the West African heat low (Figure 2d). These SLLJ variations are consistent with Fiedler *et al.* (2013), who used three-hourly, 1° ERA-Interim reanalysis and forecast data for their climatological study.

Figure 3 shows the diurnal cycle of meridional wind, zonal wind, divergence, temperature, and specific humidity at 950 hPa across 7°W–3°E during the premonsoon (AMJ) and monsoon (JAS) seasons. Each of these atmospheric variables exhibits significant diurnal variability that varies by season. During AMJ, the inland flow begins increasing at the coast (about 6°N) around 1200 UTC (Figure 3a), driven by the strong daytime temperature gradient over West Africa (Figure 3d). The low-level southerlies become further enhanced away from the coast into the early evening. There is also an early evening increase in low-level westerlies near the coast (Figure 3b), but the increase is much weaker than the meridional wind

variations. Low-level convergence over the ocean (4°N) is maximum during the late morning (Figure 3c). At 1200 UTC, low-level convergence is observed over the coastal region and propagates inland during the early afternoon at about 11 m·s^{-1}. The convergence phase speed is consistent with Grams *et al.* (2010), who estimated a sea breeze phase speed of 10 m·s^{-1} at the West African coast in boreal summer. The sea breeze front penetrates inland until 2100 UTC.

At night during AMJ, strong southerly flow (Figure 3a) and somewhat weaker westerly flow (Figure 3b) associated with the SLLJ is present around 10°N and drives low-level convergence at 15°N (Figure 3c). Our results are consistent with Parker *et al.* (2005), who showed increasing zonal winds at night when meridional winds also increase. The maximum westerly and easterly flows around 10°N and 20°N, respectively, are linked to the cyclonic circulation over the West African heat low region. Thus, the SLLJ drives low-level convergence and enhances the West African SMC at 15°N (i.e., over the Sahel) at night. However, the low specific humidity over this region (Figure 3e) inhibits convection.

Although the sea breeze and SLLJ are linked to southerly flow at similar latitude bands (i.e., between 5° and 10°N), the associated regions of low-level convergence do not interact, due to their different timing and the smaller coastal scale of the sea breeze and larger subcontinent scale of the SLLJ. The sea breeze is seen as a strong low-level convergence propagating into land (i.e., 250 km onshore) from 1200 to 1800 UTC. At 1800 UTC, the
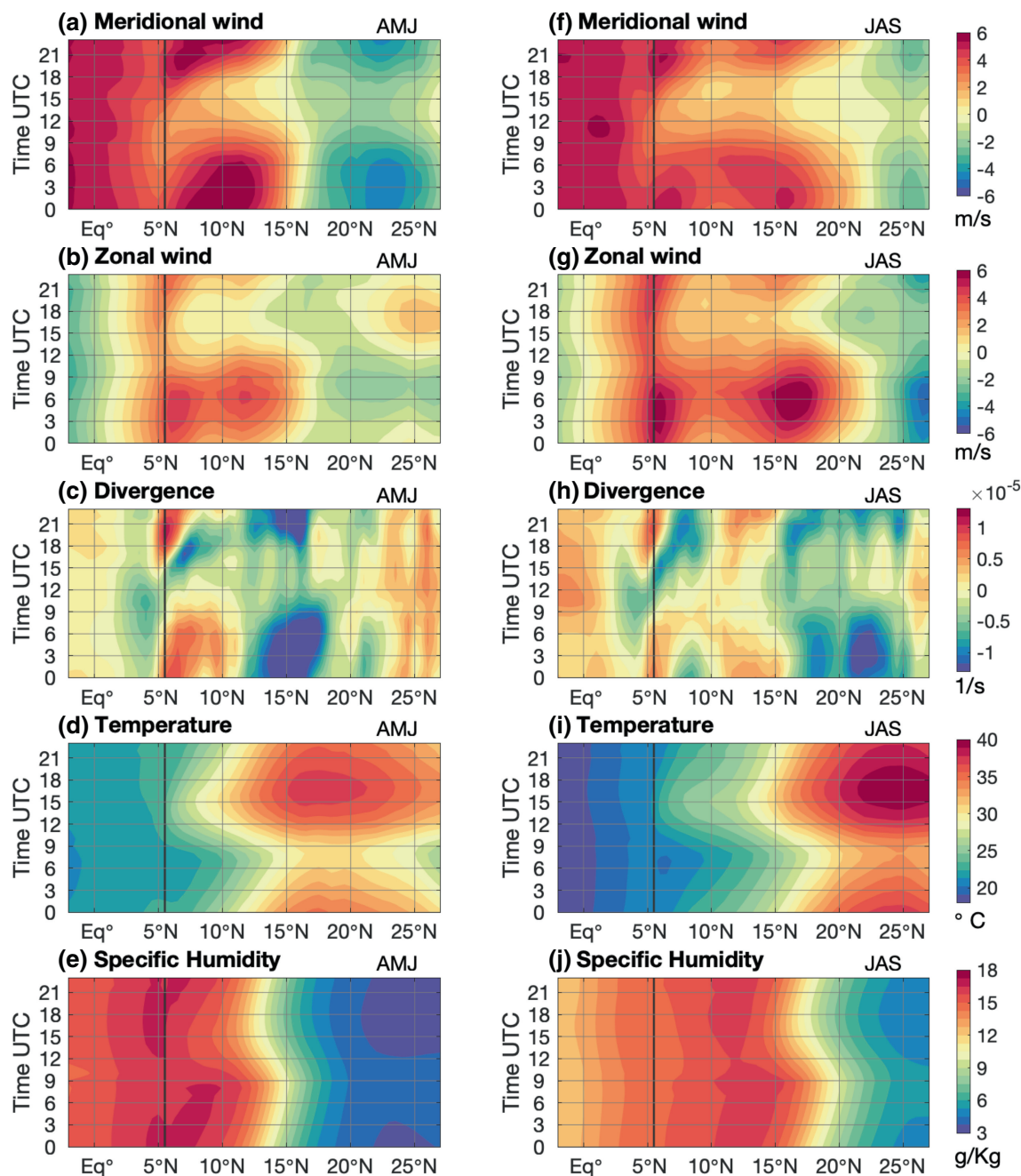
FIGURE 3 Latitude–time diagram at 950 hPa of (a,f) meridional wind in m·s^{-1}, (b,g) zonal wind in m·s^{-1}, (c,h) divergence in s^{-1}, (d,i) temperature in °C, and (e,j) specific humidity in g·kg^{-1} across 7°W–3°E during AMJ (left) and JAS (right). The solid line at 5.5°N highlights the coastline. [Colour figure can be viewed at wileyonlinelibrary.com]

maximum low-level convergence is located at 15°N (i.e., 1000 km onshore) and results from the SLLJ.

Similar to AMJ, southerly and westerly flow begins increasing at the coast around 1200 UTC during JAS (Figure 3f,g). However, the meridional flow is weaker than in AMJ because of the weaker temperature gradient near the coast (Figure 3i). The oceanic low-level convergence during JAS is maximum between 0600 and 1500 UTC (Figure 3h) and begins to propagate onshore around

1200 UTC, in association with increasing southerly flow from the Gulf of Guinea. However, the sea breeze convergence signature only propagates onshore until 1800 UTC. After 1800 UTC, a nonpropagating low-level convergence feature associated with the CLLJ is observed around 8°N until 0600 UTC, consistent with Guedje *et al.* (2019). The SLLJ is observed around 16°N (Figure 3f). While this region is now moist (Figure 3j), the SLLJ drives strong but dry low-level convergence around 21°N (Figure 3h). The
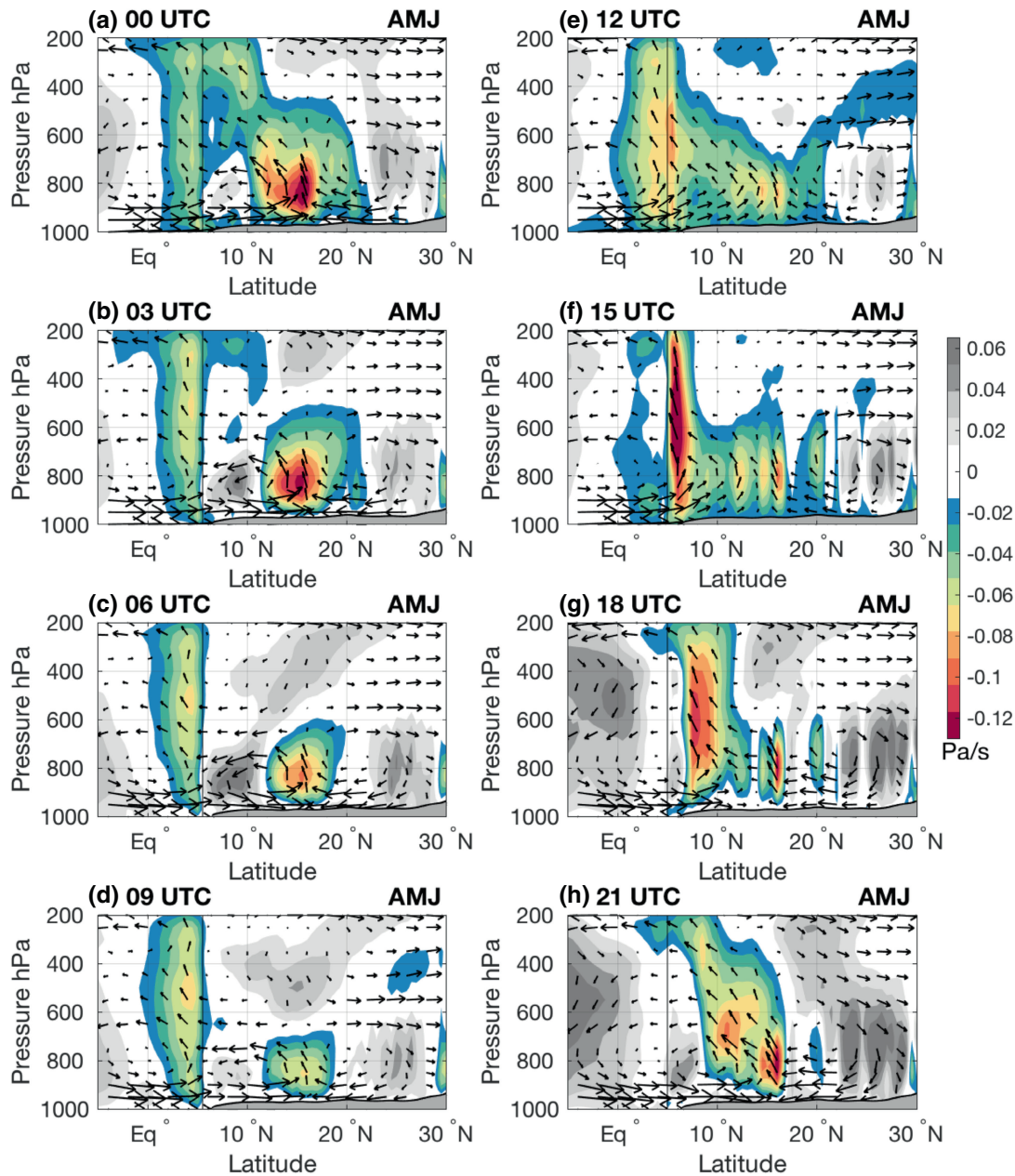
FIGURE 4 Diurnal variation of vertical motion (Pa·s⁻¹) and meridional flow cross-sections across 7°W–3°E during AMJ. The vertical meridional flow component has been multiplied by 10 to account for the small ratio of the plot. The largest meridional wind vector is 5 m·s⁻¹. The solid line at 5.5°N highlights the coastline. [Colour figure can be viewed at wileyonlinelibrary.com]

SLLJ in JAS is also less intense compared with the premonsoon season (cf. Figure 3a,f) because of the weaker southerly inflow at this higher latitude. The CLLJ does not interact with the SLLJ, which is located hundreds of km farther north.

4.2 | Meridional overturning circulations

Figures 4 and 5 show the diurnal variation in the vertical structure of the vertical velocity and meridional flow

based on ERA5 data during the premonsoon (AMJ) and monsoon (JAS) seasons, respectively. During AMJ at 0000 UTC (Figure 4a), the shallow upward motion associated with the West African SMC, with maximum overturning circulation at 800 hPa, is located at 15°N. The strong upward motion and shallow circulation are driven by the strong SLLJ, which induces low-level convergence at night (Figure 3a). Deep upward motion associated with the deep meridional circulation is seen over the ocean around 4°N. Between these two cells, there is a low-level subsidence region centered at 8°N. The subsidence may be associated
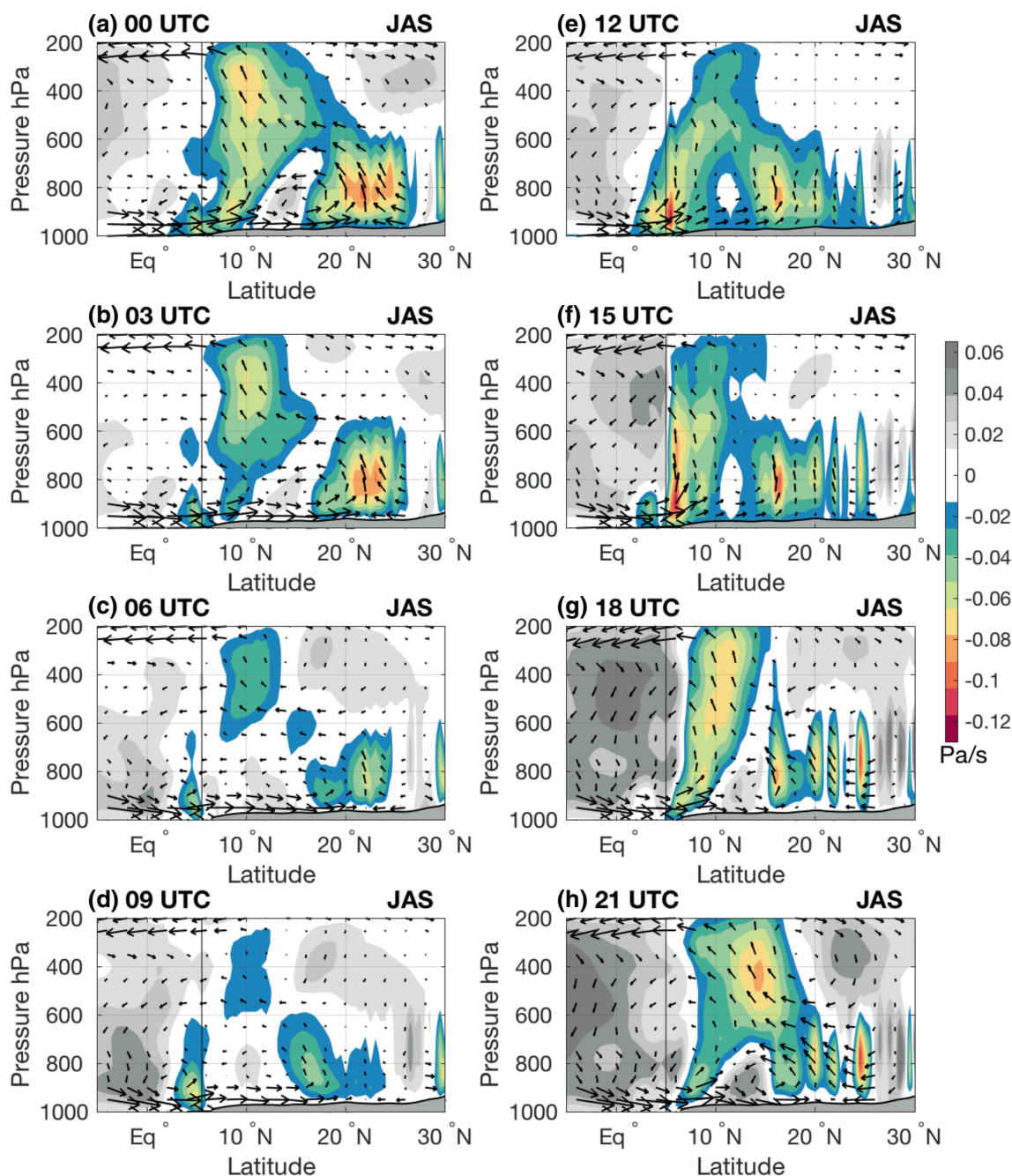
FIGURE 5   Same as Figure 4 but for JAS. [Colour figure can be viewed at wileyonlinelibrary.com]

with the stability of the PBL during nighttime and the shrinking of both planetary and relative vorticity in order to conserve the potential vorticity over this region (Vizy and Cook, 2002). A similar vertical structure is seen at 0300, 0600, and 0900 UTC (Figure 4b–d), but with the shallow upward motion weakening inland, the deep upward motion intensifying over the Gulf of Guinea, and the subsidence between the two cells strongest at 0600 UTC. The shallow upward motion over the Sahel is weakest at 0900 UTC, due to the weakening low-level convergence associated with the SLLJ after sunrise.

As daytime sensible heating warms the lower atmosphere, mixing within the PBL increases, moist air interacts with the dry near-surface air, and turbulence diffusion is generated. By 1200 UTC (Figure 4e), the subsidence at 8°N has disappeared and the deep upward motion starts to shift from the water to north over the coastal region around 6°N with the advancing sea breeze front (Figure 3a). At 1500 UTC (Figure 4f), the sea breeze front penetrates farther inland, triggering deep and strong upward motion at 7.5°N. At 1800 UTC (Figure 4g), the deep upward motion has propagated to 9°N and becomes entwined with the

southern edge of the West African SMC by 2100 UTC (Figure 4h). After the passage of the sea breeze front, advection of cool, maritime air with strong stable stratification is evident until the morning hours (Figure 3c) and the subsidence at 8°N and the SLLJ are restored.

During JAS, deep upward motion (Figure 5) and the associated precipitation (Figure 1b) are located exclusively over land, making the diurnal variation of the vertical structure of the upward motion and meridional flow over the West African region (7°W–3°E) different compared with the premonsoon season. At 0000 UTC (Figure 5a), the shallow upward motion associated with the low-level convergence driven by the SLLJ is located around 22°N, farther north and less intense compared with the premonsoon due to the weaker southerly inflow at higher latitudes. The CLLJ occurs near 8°N and also enhances shallow ascending vertical motion and probably low-level stratus clouds due to the strong low-level convergence and stratification of the boundary layer. Van der Linden *et al.* (2015) and Lohou *et al.* (2020) observed nonprecipitating, low-level clouds in the CLLJ region during nighttime. Deep upward motion is located at 10°N. The shallow and deep upward motion combined suggest a tilted monsoonal structure with shallow convection around 7°N, deep convection (i.e., ascending motion throughout the troposphere) around 9°N, and stratiform rain (i.e., ascending motion at upper levels and descending motion at lower levels) around 12°N. The low-level descending motion at 15°N is linked to the subsidence region between the deep monsoon and shallow Saharan cells, also seen during the premonsoon season during nighttime. However, whereas this descending motion strengthened during the premonsoon season between 0300 and 0600 UTC, the low-level subsidence diminishes during the monsoon season in the early morning hours (Figure 5b,c), likely because of interference from the deep cell around 10°N. This deep upward motion also weakens between 0300 and 0600 UTC, while some upper-level upward motion persists through 0900 UTC (Figure 5d). As a side note, there is oceanic shallow upward motion around 4°N, creating a shallow meridional overturning to the south related to stratus clouds typically located over the southeastern Atlantic during the early morning hours (Warren and Hahn, 2002).

At 1200 UTC (Figure 5e), the sea breeze front seems to force less deep upward motion onshore during the monsoon compared with the premonsoon (Figure 4e). Over the coast, dry conditions and descending motion predominate at mid and upper levels during the monsoon season, which inhibits deep upward motion. The sea breeze is also weaker during the monsoon, as shown in the previous section. The low-level subsidence between 10 and 15°N minimizes as the result of the air mixing in the PBL due to daytime sensible heating, similar to the premonsoon

season. At 1500 UTC (Figure 5f), the upward motion deepens and intensifies on the land side of the coast, both from the advancing sea breeze front closer to the coast and instability over a warm land surface farther away from the coast. At 1800 UTC (Figure 5g), the meridional overturning circulation is tilted with shallow upward motion around 7°N and deep upward motion around 10°N. Isolated shallow upward motion cells have developed over the Saharan region between 16° and 26°N and might be the result of the large daytime sensible heating and irregular topography over this region (Figure 1f). At 2100 UTC (Figure 5h), the monsoonal deep upward motion is located at 15°N, subsuming the southern part of the shallow cell around 18°N. Over the oceanic and coastal area, the descending motion of the deep circulation associated with the monsoon convection seems to inhibit any shallow upward motion during 1800 and 2100 UTC.

5 | DIURNAL CYCLE OF PRECIPITATION

5.1 | Total rain

The previous section showed that the diurnal cycle of vertical motion and meridional overturning over West Africa is in part forced by the sea breeze propagation, SLLJ, and CLLJ. We next analyze the the diurnal relationship between vertical motion and precipitation by season. Figure 6 shows latitude–time diagrams of the 850- and 400-hPa vertical velocity from ERA5, the precipitation and VIMD from ERA5, and the precipitation from the *TRMM/GPM* radars across 7°W–3°E during the premonsoon and monsoon season. We note that precipitation matches the midlevel ascent better than the low-level ascent patterns in most cases.

During AMJ, the 850-hPa vertical velocity (Figure 6a, contours) is similar to the near-surface convergence in Figure 3a and shows the diurnal evolution of the shallow upward motion near 15°N forced by the SLLJ during nighttime. Very little precipitation is associated with this feature in either the ERA5 (Figure 6b, shaded) or *TRMM/GPM* (Figure 6c) datasets. Over the ocean (4°N), moderate upward motion occurs throughout the troposphere (i.e., 850 and 400 hPa) at night and into the late morning and is associated with moderate rain amounts in ERA5 and strong rain amounts based on *TRMM/GPM* observations. Shallow convective rain observed by the spaceborne radars also maximizes in this region and time of day.

At 1200 UTC and over the coast during AMJ (Figure 6a), strong upward motion is seen throughout the troposphere and propagates with a phase speed around $11\,\mathrm{m\cdot s^{-1}}$ onto land during the afternoon following the
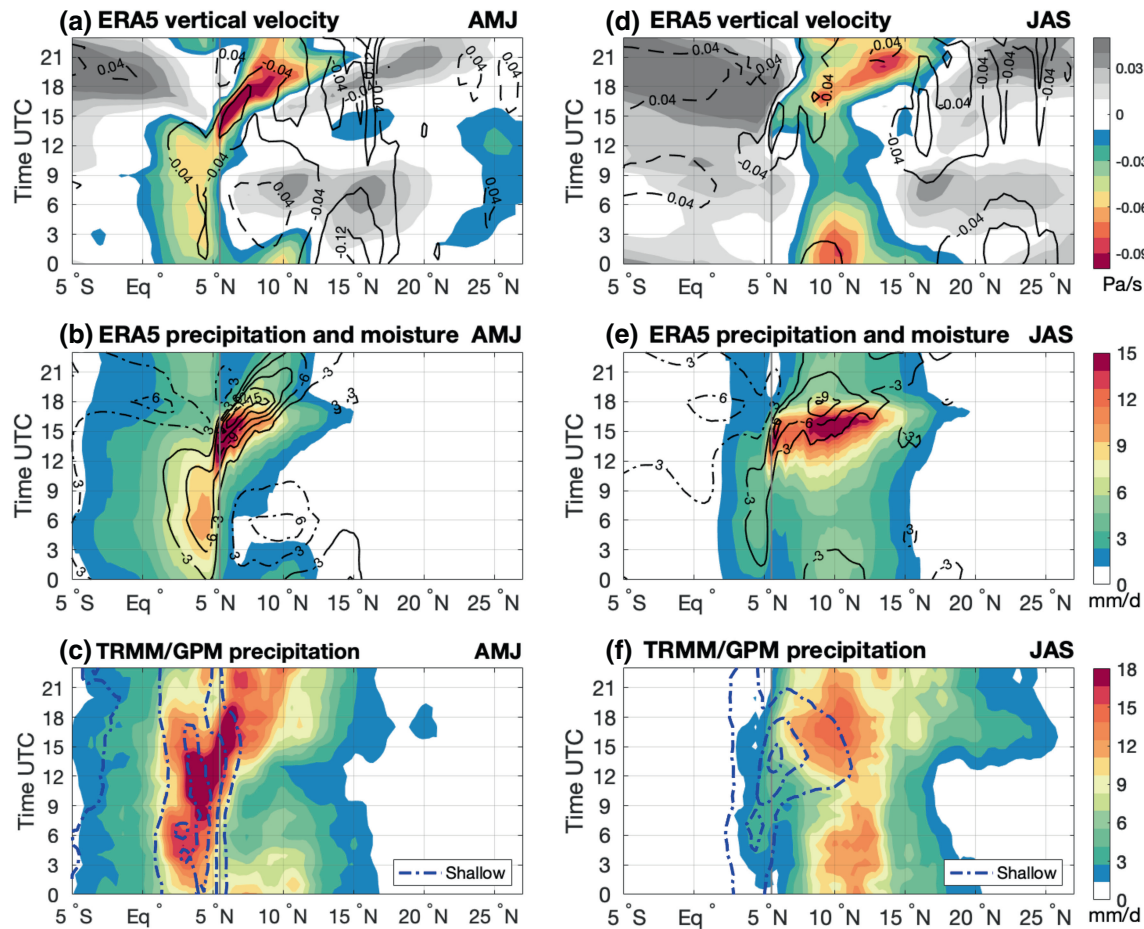
FIGURE 6 (a,d) Latitude–time diagram of vertical velocity at 400 hPa (shaded) and 850 hPa (contours) in Pa·s^{-1}, (b,e) precipitation (shaded) and VIMD (contours) in mm·day^{-1} from ERA5, and (c,f) convective (shaded), stratiform (black contours each 1 mm·day^{-1} starting at 2 mm·day^{-1}), and shallow (blue contours each 0.5 mm·day^{-1} starting at 0.5 mm·day^{-1}) precipitation in mm·day^{-1} from *TRMM–GPM*, during AMJ (left) and JAS (right). The solid gray line at 5.5°N highlights the coastline. [Colour figure can be viewed at wileyonlinelibrary.com]

sea breeze front. The propagating upward motion is associated with strong ERA5 precipitation near the coast between 1200 and 1800 UTC (Figure 6b), consistent with *TRMM/GPM* observations (Figure 6c). However, ERA5 shows low precipitation (5 mm·day^{-1}) after 1800 UTC between 6 and 12°N, while *TRMM/GPM* observes moderate precipitation (12 mm·day^{-1}) into the early morning. The ERA5 VIMD (shown as contours in Figure 6b) and precipitation maxima are collocated over the ocean, but the maximum VIMD between 8 and 10°N occurs during the early evening when ERA5 precipitation is less intense. Therefore, despite the fact that ERA5 captures the sea breeze front and its coupling to moisture, it fails to produce deep upward motion with strong precipitation between 1800 and 0000 UTC over land and instead is retrieving shallower structures with less intense precipitation but large VIMD.

During JAS, ERA5 indicates shallow upward motion over the Sahara (Figure 6d), with a nocturnal maximum around 22°N and additional regions of daytime shallow

upward motion poleward of 15°N resulting from turbulence in the PBL. ERA5 produces very little precipitation poleward of 15°N (Figure 6e), whereas *TRMM/GPM* indicates light to moderate daytime rain at these latitudes (Figure 6f). This disparity suggests that the ERA5 convective parameterization needs to be more responsive to shallow large-scale forcing, in this case the production of large eddies in the PBL resulting from strong daytime heating that can overcome environmental convective inhibition and produce deep convective cells. On the other hand, ERA5 produces larger rain amounts over the Gulf of Guinea compared with *TRMM/GPM*, despite the general absence of large-scale upward motion.

Over the coast during JAS, the sea breeze forces shallow upward motion (Figure 6d) and shallow precipitation (Figure 6f) during the early afternoon that then transitions into deeper upward motion and convection. The CLLJ, which occurs around 8°N between 1800 and 0300 UTC (Figures 2 and 3g), forces very shallow upward motion and is not linked to significant precipitation in the ERA5

(Figure 6e) or *TRMM/GPM* (Figure 6f) datasets. Therefore, low-level stratus clouds are suggested over this region. VIMD is also enhanced just to the north of the CLLJ (Figure 6e). The 400-hPa vertical velocity (Figure 6d) indicates deep upward motion from 10° to 15°N between 1500 and 0600 UTC associated with the African monsoon, which appears to be independent from the sea breeze front. Although ERA5 and *TRMM/GPM* both show inland precipitation propagation near the coast associated with the sea breeze, the precipitation datasets are inconsistent in the African monsoon region (around 10°N). ERA5 shows large precipitation amounts ($> 15 \, \text{mm·day}^{-1}$) between 1500 and 1800 UTC with a significant decrease in precipitation after 1800 UTC, while *TRMM/GPM* observes moderate precipitation (7–$10 \, \text{mm·day}^{-1}$) from the afternoon into the morning hours. ERA5 VIMD (Figure 6e) shows a similar diurnal variation compared with *TRMM/GPM* precipitation in the African monsoon region, but the ERA5 precipitation does not respond to the VIMD and large-scale vertical motion fields over land during the evening hours (similar to what occurs during AMJ). The early and overly intense onset of precipitation over land during the day is also a persistent problem in most climate models (Dai, 2006; Kniffka *et al.*, 2019; Fiedler *et al.*, 2020).

5.2 | Rain type separation

To further explore the diurnal precipitation differences between ERA5 and *TRMM/GPM*, we compare different types of precipitation from both datasets. ERA5 provides convective and large-scale precipitation, which depend on the convective and cloud microphysical schemes, respectively (Haerter and Berg, 2009). Convective precipitation is generated by the convection scheme, which represents convection at spatial scales smaller than the grid box. The cloud microphysical scheme represents the formation and dissipation of clouds and large-scale precipitation due to changes in atmospheric quantities (such as pressure, temperature and moisture) at spatial scales of the grid box. The convection scheme operates first and can affect the production of large-scale rain by affecting moisture in the grid if convection occurs during the time step. Otherwise, the large-scale microphysics is responsible for any rain production.

The *TRMM* and *GPM* radars provide convective, stratiform, and shallow precipitation that has been classified according to the vertical profile and intensity of the footprint-scale reflectivity (see Section 2). While ERA5 convective precipitation should generally be equivalent to the *TRMM/GPM* convective precipitation, ERA5 large-scale precipitation is not a physical equivalent of radar-based stratiform precipitation.

Stratiform rain represents aged convection in the Tropics (Houze, 1989; Houze, 1997); however, ERA5 diagnoses large-scale rain directly from grid-scale variables rather than via subgrid-scale convection. Regardless, comparing the precipitation types from both datasets is helpful in determining where and when the ERA5 rainfall (which is heavily model based) diverges most from the radar-observed rainfall over West Africa.

Figure 7 shows latitude–time plots of the convective and large-scale precipitation from ERA5 and convective and stratiform precipitation from *TRMM/GPM* during the premonsoon and monsoon seasons. As already discussed, ERA5 underestimates precipitation over the Gulf of Guinea (2–5°N) during AMJ compared with *TRMM/GPM* (Figure 6b,c). Figure 7a,c demonstrates that this underestimate occurs in both the convective and large-scale rain fields. While the underestimation originates with the underproduction of rain by the convective parameterization, we note that the large-scale microphysics are not sufficient to overcome this underproduction. ERA5 and *TRMM/GPM* show better agreement in the convective rain associated with the sea breeze front. The most intense convective precipitation is observed near the coast (i.e., within 200 km onshore) and both datasets are consistent in daytime propagation and intensity. However, ERA5 underestimates convective rain by about 20% during nighttime over land. The large-scale precipitation from ERA5 and stratiform precipitation *TRMM/GPM* differ more strongly over land, with almost no large-scale rain being produced by ERA5, while *TRMM/GPM* indicates that about a third of the rain is stratiform. Therefore, the ERA5 total precipitation biases during the premonsoon season are associated with the inability of the convective parameterization and large-scale microphysics scheme to represent mesoscale convective system life cycles and stratiform rain processes (e.g., Schumacher and Houze, 2003; Dai, 2006), especially at night.

During JAS, ERA5 overestimates land rainfall during the day and underestimates it at night compared with *TRMM/GPM* (Figure 6e,f). Figure 7b,d illustrates that, once again, the daytime convective precipitation signatures match reasonably well between the two datasets, this time over the broader monsoon rain band, although ERA5 1500–1800 UTC convective rain is overly intense and there continues to be less agreement in convective rain at night. In addition, the difference between the ERA5 large-scale rain and the *TRMM/GPM* stratiform rain remains stark. While ERA5 produces large-scale precipitation over land during the monsoon season (unlike during the premonsoon season), large-scale rain rates are low and maximize from 0900 to 1200 UTC, in contrast to the *TRMM/GPM* observations, which show stratiform rain rates at a minimum at 0900 UTC and largest at 1800 and 0300–0600 UTC.
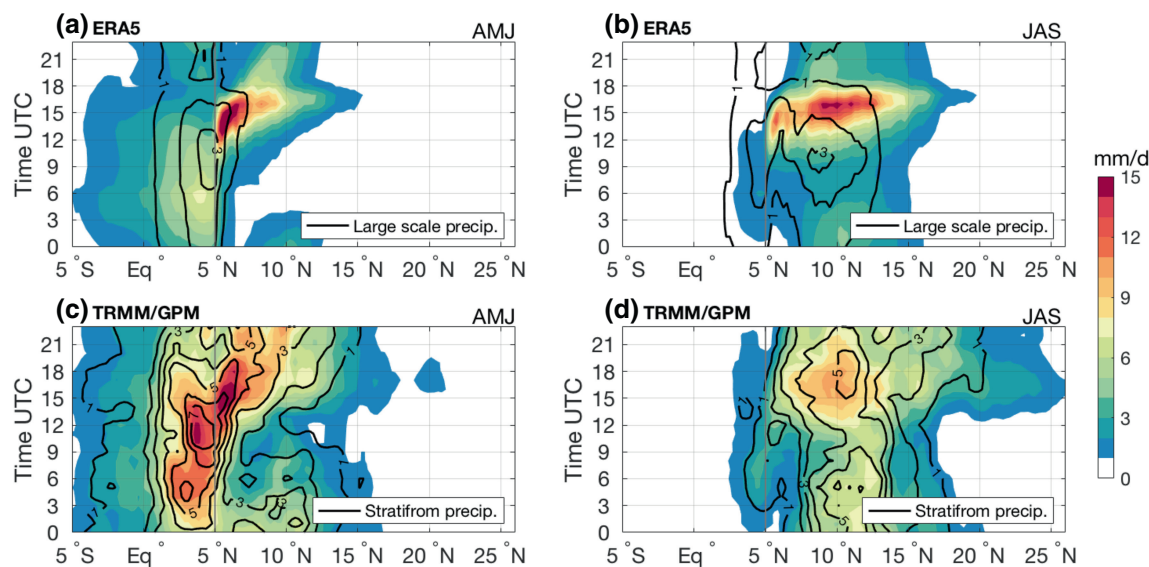
FIGURE 7   Latitude–time diagram of (a,b) convective (shaded) and large scale (contours) precipitation from ERA, and (c,d) convective plus shallow (shaded) and stratiform (contours) precipitation from *TRMM/GPM* across 7°W–3°E during AMJ. Precipitation in mm·day^{-1}. The solid gray line at 5.5°N highlights the coastline. [Colour figure can be viewed at wileyonlinelibrary.com]

The *TRMM/GPM* stratiform precipitation is also coincident with or slightly lags the convective precipitation, consistent with the concept of stratiform rain forming from regions with active convection, whereas the ERA5 large-scale rain appears to form in isolation, separate from any convective rain signal. Therefore, the ERA5 total precipitation biases during the monsoon season also result from inaccuracies in both convective and microphysical scheme performance and their inability to represent long-lived, organized convective systems.

6 | SYNTHESIS OF MERIDIONAL OVERTURNING DIURNAL MECHANISMS OVER WEST AFRICA

The purpose of this section is to synthesize the impacts of the sea breeze, SLLJ and CLLJ, and convective evolution on the meridional overturning circulations over West Africa before and during the active monsoon season. Figure 8 shows a schematic of the diurnal cycle of meridional flow, upward motion, and convection motivated by both the ERA5 dynamical fields and *TRMM/GPM* radar precipitation analyzed in the previous sections. Note that the convective structures and rainfall are based mainly on *TRMM/GPM* when disagreement exists between *TRMM/GPM* and ERA5, especially during the monsoon season (cf. Figure 6e,f).

During AMJ, a combination of shallow convective, deep convective, and stratiform rain is located over the ocean at 0900 UTC associated with both shallow and deep

overturning (Figure 8a). A region of nonprecipitating shallow upward motion is present at 15°N and is related to the low-level convergence driven by the temperature gradient in the Sahara region. Low-level subsidence is seen around 10°N between the deep and shallow overturning cells. From 1200 to 2100 UTC (Figure 8b), a southerly, maritime flow (indicated by the blue arrow) associated with the sea breeze front propagates onto land. The resulting convection is deep and produces strong convective and stratiform precipitation and a deep daytime overturning cell over land. While the deep convection propagates inland, the weakly precipitating shallow convection stays over the ocean and eventually dies off. Mixing in the PBL due to sensible heating (yellow arrow) helps enhance daytime convection and inhibits the shallow overturning cell. By 2100 UTC, the AMJ convection reaches the southern part of the West African SMC. Between 0000 and 0600 UTC (Figure 8c), the convection over land has died out completely and new convection forms over the ocean. The mixing layer over the PBL has vanished and strong shallow descending motion reemerges between the shallow and deep cells around 10°N. The SLLJ (indicated by the red arrow) develops during this time and strengthens the SMC over the Sahel due to strong low-level convergence with the synoptic-scale northerlies.

During JAS, a different diurnal cycle in low-level wind features, convection, and meridional overturning is seen. At 0900 UTC (Figure 8d), shallow precipitating convection is present over the ocean and dry shallow upward motion associated with the West African heat low occurs at 20°N. However, the SMC is weaker than during the premonsoon
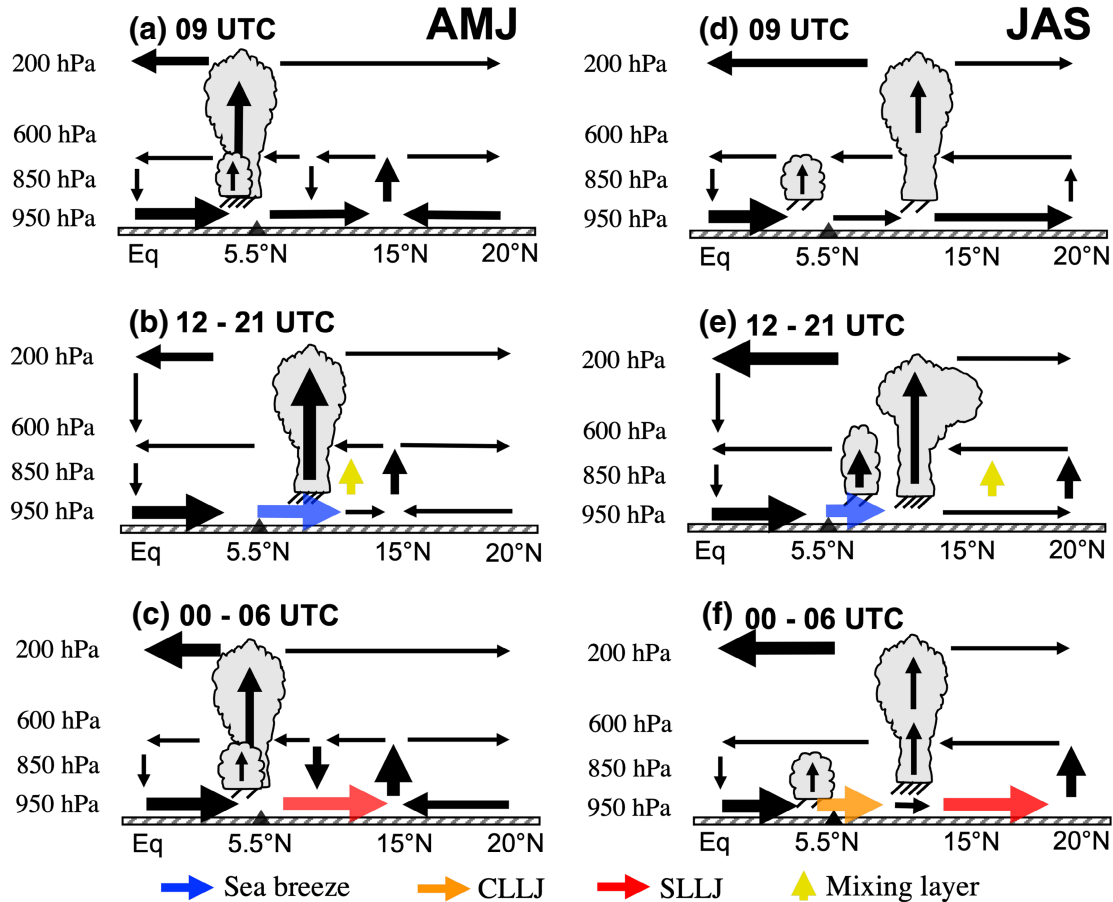
FIGURE 8   Schematic of the diurnal variation of West African meridional overturning and convection during the premonsoon (left) and monsoon (right) season. The triangle indicates the location of the coastline. The thin, thick, and thickest horizontal (vertical) vectors indicate meridional winds (upward motion) smaller than $2\,\text{m·s}^{-1}$ ($-0.05\,\text{Pa·s}^{-1}$), between 2 and $4\,\text{m·s}^{-1}$ (-0.05 and $-0.1\,\text{Pa·s}^{-1}$), and larger than $4\,\text{m·s}^{-1}$ ($-0.1\,\text{Pa·s}^{-1}$), respectively. Two (four) dashes under the convective cloud indicate precipitation smaller (larger) than $18\,\text{mm·day}^{-1}$ during the premonsoon season and smaller (larger) than $13\,\text{mm·day}^{-1}$ during the monsoon season. [Colour figure can be viewed at wileyonlinelibrary.com]

and does not have a strong descending branch to the south. A mix of deep convective and stratiform rain is present around 12°N, but the predominance of the stratiform rain (more likely to occur in the decaying phase of large convective systems) causes the large-scale vertical velocity to be top-heavy. From 1200 to 2100 UTC (Figure 8e), newly developing deep precipitating convection associated with daytime heating over land is located near 10°N and is independent of the shallower convection in the coastal region forced by the sea breeze front. The inland convection is strongest at these times, producing a strong deep meridional overturning, while the less deep convection from the coast vanishes by 2100 UTC. Between 0000 and 0600 UTC (Figure 8f), two strong low-level southerly flows are seen over land and are linked to the CLLJ and SLLJ. The CLLJ (orange arrow) is important for the northward transport of moisture that helps maintain the organized convective systems and deep meridional overturning over land at night. The deep convection eventually decays

and precipitating midlevel clouds are observed, consistent with *CloudSat* data (Stein *et al.*, 2011). Low-level stratus clouds are observed at night closer to the coast (Lohou *et al.*, 2020) and are related to the CLLJ. The SLLJ and associated low-level convergence have intensified the shallow upward and downward motion associated with the West African SMC.

7 | SUMMARY AND CONCLUSIONS

We used ERA5 reanalysis and *TRMM* and *GPM* satellite radar data from 1998 to 2019 to provide new insights on the West African shallow and deep meridional overturning during the premonsoon (AMJ) and monsoon (JAS) seasons. The newest piece was to explain the diurnal cycle of the meridional overturning circulations, which until now had only been presented as seasonal means. We showed that there are very large changes in the shallow

and deep meridional overturning throughout the day and that these variations are dependent on the existence and strength of low-level wind features such as the sea breeze and nocturnal low-level jets. Convective evolution and structure also play a role in the meridional overturning characteristics.

ERA5 dynamical fields showed evidence of a sea breeze and low-level jets in the afternoon and nighttime, respectively, consistent with previous observational studies (Lothon *et al.*, 2008; Guedje *et al.*, 2019; Lohou *et al.*, 2020). The sea breeze front forces low-level convergence that triggers convective systems and assists in their propagation from the coast inland. The sea breeze penetrates farther inland once turbulence in the PBL dies down in the evening. This is likely what Lohou *et al.* (2020) called the "maritime inflow" that arrived at Savè (Benin), almost 200 km inland of the Guinea Coast, between 1600 and 2000 UTC. The sea breeze is stronger in the premonsoon season and produces deeper, more intense convection that travels farther inland compared with the monsoon season. However, the deep meridional overturning is similar during the day between the two seasons because of the inland environment during the monsoon (i.e., a warm, moist, well-mixed lower troposphere), which is conducive to producing deep convection beyond the extent reached by the sea breeze. Weak SMCs are present during the day during both seasons, but they do not have distinct descending branches to the south; rather, their return flow enters the deep convective regions at multiple levels and their southern edge becomes entangled with the deep overturning by 2100 UTC.

While deep meridional overturning does not persist over land at night during the premonsoon, the CLLJ is clearly discernible in ERA5 during JAS and provides a source of inland moisture that helps maintain convective systems with large stratiform rain regions and top-heavy meridional overturning over night during the monsoon. Shallow precipitating convection near the coast produces small overturning cells over the ocean at night during both seasons, but the main nocturnal shallow meridional overturning circulation occurs farther north: over the Sahel in AMJ and over the Sahara in JAS. The evolution of the West African SMC is driven by the SLLJ, which forces low-level convergence over the West African heat low, enhancing the dry SMC throughout the year (Parker *et al.*, 2005). The associated dry shallow upward motion intensifies during nighttime when the PBL is stratified and wind shear is weak and a distinct descending branch occurs before reaching the region of deep overturning. It remains an open question whether a stronger SMC can enhance or hinder deep convection to the south (e.g., Martin and Thorncroft, 2014; Shekhar and Boos, 2017); however, our results indicate that diurnal variations must

be considered because the interactions between deep and shallow meridional overturning vary throughout the diurnal cycle over West Africa.

TRMM/*GPM* and ERA5 precipitation were also compared. ERA5 has a small precipitation bias over the coastal region, where the sea breeze front plays an important role in triggering convection during the early afternoon. However, ERA5 strongly underestimates precipitation over the Gulf of Guinea during the premonsoon and farther inland during the monsoon, when each region is experiencing large rain amounts. This underestimation occurs in both the convective and large-scale rain fields, so fixing the underestimation would require assessment of the convective parameterization, the large-scale microphysics, and their interaction. Although ERA5 shows biases in the diurnal cycle of precipitation, it is able to capture many of the dynamical features associated with the diurnal low-level circulation features over West Africa, like the sea breeze and nocturnal low-level jets. Sensitivity tests (not shown) indicate that ERA5 performs better than other reanalyses in capturing these features. Therefore, we consider ERA5 to be an appropriate reanalysis to study the diurnal variation of the West African meridional overturning, but its precipitation should be complemented by observational sources due to limitations in the ERA5 convective and microphysical schemes in simulating mesoscale organized convection. In this context, the latest change to the convective parameterization scheme in the ECMWF forecast model as described in Becker *et al.* (2021), which improved the convective organization in West Africa substantially, has the potential to reduce the deficiencies in model precipitation.

AUTHOR CONTRIBUTIONS

Lidia Huaman: data curation; formal analysis; investigation; methodology; visualization; writing – original and draft. **Courtney Schumacher:** conceptualization; funding acquisition; supervision; writing – review and editing. **Andreas H. Fink:** conceptualization; funding acquisition; investigation; writing – review and editing. **Erin Buttitta:** investigation.

ACKNOWLEDGEMENTS

DATA AVAILABILITY STATEMENT

ORCID

Lidia Huaman https://orcid.org/0000-0002-9812-9587
Courtney Schumacher https://orcid.org/0000-0003-3612-485X
Andreas H. Fink https://orcid.org/0000-0002-5840-2120

REFERENCES

Adirosi, E., Montopoli, M., Bracci, A., Porcu, F., Capozzi, V., Annella, C., Budillon, G., Bucchignani, E., Zollo, A.L., Cazzuli, O. and Camisani, G. (2021) Validation of GPM rainfall and drop size distribution products through disdrometers in Italy. *Remote Sensing*, 13(11), 2081.

Atiah, W.A., Amekudzi, L.K., Aryee, J.N.A., Preko, K. and Danuor, S.K. (2020) Validation of satellite and merged rainfall data over Ghana, West Africa. *Atmosphere*, 11(8), 859.

Awaka, J., Iguchi, T. and Ken'ichi, O. (2007) Rain type classification algorithm. In: *Measuring Precipitation from Space*. Springer, pp. 213–224. https://link.springer.com/chapter/10.1007/978-1-4020-5835-6_17

Becker, T., Bechtold, P. and Sandu, I. (2021) Characteristics of convective precipitation over tropical Africa in storm-resolving global simulations. *Quarterly Journal of the Royal Meteorological Society*, 147(741), 4388–4407.

Bouniol, D., Couvreux, F., Kamsu-Tamo, P.-H., Leplay, M., Guichard, F., Favot, F. and O'Connor, E.J. (2012) Diurnal and seasonal cycles of cloud occurrences, types, and radiative impact over West Africa. *Journal of Applied Meteorology and Climatology*, 51(3), 534–553.

Cannon, F., Ralph, F.M., Wilson, A.M. and Lettenmaier, D.P. (2017) GPM satellite radar measurements of precipitation and freezing level in atmospheric rivers: comparison with ground-based radars and reanalyses. *Journal of Geophysical Research: Atmospheres*, 122(23), 12–747.

Collow, A.B., Ghate, V.P., Miller, M.A. and Trabachino, L.C. (2016) A one-year study of the diurnal cycle of meteorology, clouds and radiation in the west African Sahel region. *Quarterly Journal of the Royal Meteorological Society*, 142(694), 16–29.

Dai, A. (2006) Precipitation characteristics in eighteen coupled climate models. *Journal of Climate*, 19(18), 4605–4630.

Dembélé, M. and Zwart, S.J. (2016). Evaluation and comparison of satellite-based rainfall products in Burkina Faso, West Africa. *International Journal of Remote Sensing*, 37(17), 3995–4014.

Diro, G.T., Rauscher, S.A., Giorgi, F. and Tompkins, A.M. (2012) Sensitivity of seasonal climate and diurnal precipitation over Central America to land and sea surface schemes in RegCM4. *Climate Research*, 52, 31–48.

Fiedler, S., Crueger, T., D'Agostino, R., Peters, K., Becker, T., Leutwyler, D., Paccini, L., Burdanowitz, J., Buehler, S.A. and Cortes, A.U. (2020) Simulated tropical precipitation assessed across three major phases of the coupled model intercomparison project (CMIP). *Monthly Weather Review*, 148(9), 3653–3680.

Fiedler, S., Schepanski, K., Heinold, B., Knippertz, P. and Tegen, I. (2013) Climatology of nocturnal low-level jets over North Africa and implications for modeling mineral dust emission. *Journal of Geophysical Research: Atmospheres*, 118(12), 6100–6121.

Fink, A.H., Engel, T., Ermert, V., van der Linden, R., Schneidewind, M., Redl, R., Afiesimama, E., Thiaw, W.M., Yorke, C. and Evans, M. (2017) Mean climate and seasonal cycle. In: *Meteorology of Tropical West Africa: The Forecasters' Handbook*. Wiley-Blackwell, pp. 1–39. https://onlinelibrary.wiley.com/doi/10.1002/9781118391297.ch1

Fink, A.H., Paeth, H., Ermert, V., Pohle, S. and Diederich, M. (2010) I-5.1 meteorological processes influencing the weather and climate of Benin.

Foli, B.A., Appeaning Addo, K., Ansong, J.K. and Wiafe, G. (2022) Evaluation of ECMWF and NCEP reanalysis wind fields for long-term historical analysis and ocean wave modelling in West Africa. *Remote Sensing in Earth Systems Sciences*, 5(1-2), 26–45.

Funk, A. (2013) Courtney Schumacher, and Jun Awaka. Analysis of rain classifications over the tropics by version 7 of the TRMM PR 2a23 algorithm. *Journal of the Meteorological Society of Japan. Series II*, 91(3), 257–272.

Gounou, A., Guichard, F. and Couvreux, F. (2012) Observations of diurnal cycles over a west african meridional transect: pre-monsoon and full-monsoon seasons. *Boundary-Layer Meteorology*, 144(3), 329–357.

Grams, C.M., Jones, S.C., Marsham, J.H., Parker, D.J., Haywood, J.M. and Heuveline, V. (2010) The Atlantic inflow to the Saharan heat low: observations and modelling. *Quarterly Journal of the Royal Meteorological Society*, 136(1), 125–140.

Gu, G. and Adler, R.F. (2004) Seasonal evolution and variability associated with the west African monsoon system. *Journal of Climate*, 17(17), 3364–3377.

Guedje, F.K., Houeto, A.V.V., Houngninou, E.B., Fink, A.H. and Knippertz, P. (2019) Climatology of coastal wind regimes in Benin. *Meteorologische Zeitschrift*, 28, 23–39.

Haerter, J.O. and Berg, P. (2009) Unexpected rise in extreme precipitation caused by a shift in rain type? *Nature Geoscience*, 2(6), 372–373.

Hagos, S. and Zhang, C. (2010) Diabatic heating, divergent circulation and moisture transport in the African monsoon system. *Quarterly Journal of the Royal Meteorological Society*, 136(1), 411–425.

Hall, N.M. and Peyrille, P. (2006) Dynamics of the west African monsoon. Proceedings Journal de Physique IV, EDP sciences. Vol. 139, pp. 81-99.

Hersbach, H., Bell, B., Berrisford, P., Hirahara, S., Horányi, A., Muñoz-Sabater, J., Nicolas, J., Peubey, C., Radu, R. and Schepers, D. (2020) The ERA5 global reanalysis. *Quarterly Journal of the Royal Meteorological Society*, 146, 1999–2495.

Hou, A.Y., Kakar, R.K., Neeck, S., Azarbarzin, A.A., Kummerow, C.D., Kojima, M., Oki, R., Nakamura, K. and Iguchi, T. (2014) The global precipitation measurement mission. *Bulletin of the American Meteorological Society*, 95(5), 701–722.

Houze, R.A. (1989) Observed structure of mesoscale convective systems and implications for large-scale heating. *Quarterly Journal of the Royal Meteorological Society*, 115(487), 425–461.

Houze, R.A. (1997) Stratiform precipitation in regions of convection: a meteorological paradox? *Bulletin of the American Meteorological Society*, 78(10), 2179–2196.

Huaman, L. and Schumacher, C. (2018) Assessing the vertical latent heating structure of the East Pacific ITCZ using the CloudSat CPR and TRMM PR. *Journal of Climate*, 31(7), 2563–2577.

Janiga, M.J. and Thorncroft, C.D. (2014) Convection over tropical Africa and the East Atlantic during the west African monsoon: regional and diurnal variability. *Journal of Climate*, 27(11), 4159–4188.

Johnson, R.H. and Ciesielski, P.E. (2020) Potential vorticity generation by west African squall lines. *Monthly Weather Review*, 148(4), 1691–1715.

Kniffka, A., Knippertz, P. and Fink, A.H. (2019) The role of low-level clouds in the west African monsoon system. *Atmospheric Chemistry and Physics*, 19(3), 1623–1647.

Kodama, Y., Katsumata, M., Mori, S., Satoh, S., Hirose, Y. and Ueda, H. (2009) Climatology of warm rain and associated latent heating derived from TRMM PR observations. *Journal of Climate*, 22(18), 4908–4929.

Kummerow, C., Barnes, W., Kozu, T., Shiue, J. and Simpson, J. (1998) The tropical rainfall measuring mission (TRMM) sensor package. *Journal of Atmospheric and Oceanic Technology*, 15(3), 809–817.

Laing, A.G., Carbone, R., Levizzani, V. and Tuttle, J. (2018) The propagation and diurnal cycles of deep convection in northern tropical Africa. *Quarterly Journal of the Royal Meteorological Society: A Journal of the Atmospheric Sciences, Applied Meteorology and Physical Oceanography*, 134(630), 93–109.

Lavaysse, C., Flamant, C., Janicot, S., Parker, D.J., Lafore, J.-P., Sultan, B. and Pelon, J. (2009) Seasonal evolution of the west African heat low: a climatological perspective. *Climate Dynamics*, 33(2-3), 313–330.

Liu, W., Cook, K.H. and Vizy, E.K. (2019) The role of mesoscale convective systems in the diurnal cycle of rainfall and its seasonality over sub-saharan northern Africa. *Climate Dynamics*, 52(1), 729–745.

Liu, W., Cook, K.H. and Vizy, E.K. (2020) Role of the west African westerly jet in the seasonal and diurnal cycles of precipitation over West Africa. *Climate Dynamics*, 54(1), 843–861.

Lohou, F., Kalthoff, N., Adler, B., Babić, K., Dione, C., Lothon, M., Pedruzo-Bagazgoitia, X. and Zouzoua, M. (2020) Conceptual model of diurnal cycle of low-level stratiform clouds over southern West Africa. *Atmospheric Chemistry and Physics*, 20(4), 2263–2275.

Lothon, M., Saïd, F., Lohou, F. and Campistron, B. (2008) Observation of the diurnal cycle in the low troposphere of West Africa. *Monthly Weather Review*, 136(9), 3477–3500.

Maranan, M., Fink, A.H. and Knippertz, P. (2018) Rainfall types over southern West Africa: objective identification, climatology and synoptic environment. *Quarterly Journal of the Royal Meteorological Society*, 144(714), 1628–1648.

Martin, E.R. and Thorncroft, C.D. (2014) The impact of the AMO on the west African monsoon annual cycle. *Quarterly Journal of the Royal Meteorological Society*, 140(678), 31–46.

Nesbitt, S.W. and Zipser, E.J. (2003) The diurnal cycle of rainfall and convective intensity according to three years of TRMM measurements. *Journal of Climate*, 16(10), 1456–1475.

Parker, D.J., Burton, R.R., Diongue-Niang, A., Ellis, R.J., Felton, M., Taylor, C.M., Thorncroft, C.D., Bessemoulin, P. and Tompkins, A.M. (2005) The diurnal cycle of the west African monsoon circulation. *Quarterly Journal of the Royal Meteorological Society*, 131(611), 2839–2860.

Pfeifroth, U., Trentmann, J., Fink, A.H. and Ahrens, B. (2016) Evaluating satellite-based diurnal cycles of precipitation in the African tropics. *Journal of Applied Meteorology and Climatology*, 55(1), 23–39.

Schumacher, C. and Houze Jr, R.A. (2006) Stratiform precipitation production over sub-Saharan Africa and the tropical East Atlantic as observed by TRMM. *Quarterly Journal of the Royal Meteorological Society*, 132(620), 2235–2255.

Schumacher, C. and Houze, R.A. (2003) Stratiform rain in the tropics as seen by the TRMM precipitation radar. *Journal of Climate*, 16(11), 1739–1756.

Shekhar, R. and Boos, W.R. (2017) Weakening and shifting of the saharan shallow meridional circulation during wet years of the west african monsoon. *Journal of Climate*, 30(18), 7399–7422.

Stein, T.H., Parker, D.J., Julien Delanoë, N.S., Dixon, R.J., Hogan, P.K., Maidment, R.I. and Marsham, J.H. (2011) The vertical cloud structure of the west African monsoon: a 4 year climatology using CloudSat and CALIPSO. *Journal of Geophysical Research: Atmospheres*, 116(D22). https://agupubs.onlinelibrary.wiley.com/doi/epdf/10.1029/2011JD016029

Steiner, M., Houze Jr, R.A. and Yuter, S.E. (1995) Climatological characterization of three-dimensional storm structure from operational radar and rain gauge data. *Journal of Applied Meteorology*, 34(9), 1978–2007.

Stocker, E.F., Alquaied, F., Bilanow, S., Ji, Y. and Jones, L. (2018) TRMM version 8 reprocessing improvements and incorporation into the GPM data suite. *Journal of Atmospheric and Oceanic Technology*, 35(6), 1181–1199.

Sultan, B., Janicot, S. and Drobinski, P. (2007) Characterization of the diurnal cycle of the west African monsoon around the monsoon onset. *Journal of Climate*, 20(15), 4014–4032.

Thorncroft, C.D. and Blackburn, M. (1999) Maintenance of the African easterly jet. *Quarterly Journal of the Royal Meteorological Society*, 125(555), 763–786.

Thorncroft, C.D., Nguyen, H., Zhang, C. and Peyrillé, P. (2011) Annual cycle of the west African monsoon: regional circulations and associated water vapour transport. *Quarterly Journal of the Royal Meteorological Society*, 137(654), 129–147.

Trenberth, K.E., Stepaniak, D.P. and Caron, J.M. (2000) The global monsoon as seen through the divergent atmospheric circulation. *Journal of Climate*, 13(22), 3969–3993.

Van der Linden, R., Fink, A.H. and Redl, R. (2015) Satellite-based climatology of low-level continental clouds in southern West Africa during the summer monsoon season. *Journal of Geophysical Research: Atmospheres*, 120(3), 1186–1201.

Vizy, E.K. and Cook, K.H. (2002) Development and application of a mesoscale climate model for the tropics: influence of sea surface temperature anomalies on the west African monsoon. *Journal of Geophysical Research: Atmospheres*, 107(D3), ACL-2.

Vizy, E.K. and Cook, K.H. (2019) Understanding the summertime diurnal cycle of precipitation over sub-saharan west Africa: regions with daytime rainfall peaks in the absence of significant topographic features. *Climate Dynamics*, 52(5), 2903–2922.

Vondou, D.A., Nzeukou, A., Lenouo, A., Mkankam, K.F. (2010) Seasonal variations in the diurnal patterns of convection in

Cameroon–Nigeria and their neighboring areas. *Atmospheric Science Letters*, 11(4), 290–300.

Warren, S.G. and Hahn, C.J. (2002) *Clouds/Climatology*. Encyclopedia of Atmospheric Sciences. https://atmos.uw.edu/~sgw/PAPERS/2014_cloud_encyclopedia.pdf

Yang, G. and Slingo, J. (2001) The diurnal cycle in the tropics. *Monthly Weather Review*, 129(4), 784–801.

Zhang, C., Nolan, D.S., Thorncroft, C.D. and Nguyen, H. (2008) Shallow meridional circulations in the tropical atmosphere. *Journal of Climate*, 21(14), 3453–3470.

Zhang, C., Woodworth, P. and Guojun, G. (2006) The seasonal cycle in the lower troposphere over west africa from sounding observations. *Quarterly Journal of the Royal Meteorological Society: A Journal of the Atmospheric Sciences, Applied Meteorology and Physical Oceanography*, 132(621), 2559–2582.

Zhang, G., Cook, K.H. and Vizy, E.K. (2016) The diurnal cycle of warm season rainfall over West Africa. Part i: observational analysis. *Journal of Climate*, 29(23), 8423–8437.